The effect of Dean, Reynolds and Womersley numbers on the flow in a spherical cavity on a curved round pipe. Part 2. The haemodynamics of intracranial aneurysms treated with flow-diverting stents

Michael C Barbour, Fanette Chassagne, Nathanaël Machicoane, Venkat K Chivukula, Louis J Kim, Michael R Levitt, Alberto Aliseda

The effect of Dean, Reynolds, and Womersley number on the flow in a spherical cavity on a curved round pipe. Part 2: The hemodynamics of intracranial aneurysms treated with flow-diverting stents.

Michael C. Barbour[1]††, Fanette Chassagne[1]†, Nathanael Machicoane[4], Venkat K. Chivukula[5], Louis J. Kim[2,3], Michael R. Levitt[1,2,3], and Alberto Aliseda[1,2]

† These authors contributed equally to this paper

[1]Department of Mechanical Engineering, University of Washington, Seattle, WA 98107, USA

[2]Department of Neurological Surgery, University of Washington, Seattle, WA 98107, USA

[3]Department of Radiology, University of Washington, Seattle, WA 98107, USA

[4]University Grenoble Alpes, CNRS, Grenoble-INP, LEGI, F-38000, Grenoble, France

[5]Biomedical and Chemical Engineering and Sciences, Florida Institute of Technology, Melbourne, FL 32901, USA

(Received xx; revised xx; accepted xx)

The flow in a spherical cavity on a curved round pipe is a canonical flow that describes well the flow inside a sidewall aneurysm on an intracranial artery. Intracranial aneurysms are often treated with a flow-diverting stent (FDS), a low porosity metal mesh that covers the entrance to the cavity, to reduce blood flow into the aneurysm sac and exclude it from mechanical stresses imposed by the blood flow. Successful treatment is highly dependent on the degree of reduction of flow inside the cavity, and the resulting altered fluid mechanics inside the aneurysm following treatment. Using stereo-PIV, we characterize the fluid mechanics in a canonical configuration representative of an intracranial aneurysm treated with FDS: a spherical cavity on the side of a curved round pipe covered with a metal mesh formed by an actual medical flow-diverting stent. This porous mesh coverage is the focus of Part 2 of the paper, characterizing the effects of parent vessel Re, De, and pulsatility, Wo, on the fluid dynamics, compared to the canonical configuration with no impediments to flow into the cavity that are described in Part 1. Coverage with a FDS drastically reduces the flow Reynolds number in the aneurysmal cavity, creating a viscous-dominated flow environment despite the parent vessel Re >100. Under steady flow-conditions, the topology that forms inside the cavity is shown to be a function of the parent vessel De. At low values of De, flow enters the cavity at the leading edge and remains attached to the wall before exiting at the trailing edge, a novel behavior that was not found under any conditions of the high Reynolds number, unimpeded, cavity flow described in Part 1. Under these conditions, flow in the cavity co-rotates with the direction of the freestream flow, similar to Stokes flow in a cavity. As the De increases, the flow along the leading edge begins to separate, and the recirculation zone grows with increasing De, until, above a $De \approx 180$, the flow inside the cavity is fully recirculating, counter-rotating with respect to the freestream flow. Under pulsatile flow conditions, the vortex inside the cavity progresses through the same cycle - switching from attached

† Email address for correspondence: barbourm@u.washington.edu

and co-rotating with the freestream flow at the beginning of the cycle (low velocity and positive acceleration), to separated and counter-rotating as the Dean number reaches a critical value. The location of separation within the harmonic cycle is shown to be a function of both De and Wo.

The aneurysmal cavity Reynolds numbers based on both the average velocity and the circulation inside the cavity are shown to increase with increasing values of De, while Wo is shown to have little influence on the time-averaged metrics. As the De increases, the strength of the secondary flow in the parent vessel grows, due to the inertial instability in the curved pipe, and the flow rate entering the cavity increases. Thus, the effectiveness of FDS treatment to exclude the aneurysmal cavity from the hemodynamic stresses is compromised for aneurysms located on high curvature arteries, i.e. vessels with high De, and this can be a fluid mechanics criterion to guide treatment selection.

Key words: Cerebral aneurysms, Flow-diverting stents, Hemodynamics, Dean number, Reynolds number, Womersely number

1. Introduction

Intracranial aneurysms are pathological outgrowths of the walls of intracranial arteries. These "berry-like" outpouches can be approximated as spherical cavities that develop on the sidewall of curved arteries that feed oxygenated blood to the brain, due to abnormal remodeling of the vascular wall (Lasheras 2007). Due to the risk of aneurysm rupture, which results in subarachnoid hemorrhage and hemorrhagic stroke with mortality rates as high as 50 % (Johnston *et al.* 1998), the pathological flow inside the cavity is treated to produce stagnation and a stable thrombus. One of two key endovascular treatment options consists of placing a low-porosity metal mesh (flow diverting stent, FDS) across the cavity opening. In practice, this is done by introducing the metal mesh cylinder through an endovascular catheter and placing it along the wall of the parent vessel covering the aneurysmal neck (the opening that communicates the parent vessel lumen to the cavity of the aneurysm). This treatment is designed to place a hydrodynamic resistance to flow entering the cavity, reducing flow velocity and stresses inside the aneurysm sac, thus encouraging remodeling in the parent vessel that redirects blood flow away from the aneurysm and creates an environment that promotes the development of a stable thrombus inside the aneurysmal sac. Unfortunately, in 20 - 25% of cerebral aneurysms treated with an FDS, complete stasis inside the aneurysmal sac does not occur, blood flow still enters the aneurysm, and thrombotic filling of the cavity is not complete, leaving the patient at risk of rupture (Brinjikji *et al.* 2013; Adeeb *et al.* 2017; Maragkos *et al.* 2020). The fluid mechanics inside the cavity after covering the opening that communicates the parent vessel with the aneurysmal sac with the porous mesh plays a crucial role in treatment success. Understanding and characterizing this fluid mechanical environment is a necessary part of improving the rate of intracranial aneurysm treatment success (Sforza *et al.* 2009; Cebral & Raschi 2013; Meng *et al.* 2014).

Investigation into the altered fluid mechanics of FDS-treated cerebral aneurysms started with the work of Lieber *et al.* (1997) and Aenis *et al.* (1997). Using planar laser induced fluorescence and computational fluid dynamics simulations respectively, both of these groups measured a significant reduction in intra-aneurysmal flow vorticity and velocity following FDS deployment, suggesting that flow stasis was enhanced by

treatment, and would likely lead to thrombus formation inside the aneurysmal sac. Since then, a number of studies (Cantón *et al.* 2005*a*,*b*; Babiker *et al.* 2012; Rayepalli *et al.* 2013; Damiano *et al.* 2015), have investigated the influence of the stent properties on aneurysmal flow reduction, attempting to determine the ideal porosity, placement location and number of stents for aneurysm flow reduction. Additionally, in recent years, much research has been focused on developing a causal relationship between reduction in aneurysm hemodynamics following FDS deployment and treatment outcome (Kulcsár *et al.* 2012; McAuliffe *et al.* 2012; Paliwal *et al.* 2017; Chen *et al.* 2019; Su *et al.* 2020). These studies have all compared changes in pre- and post-treatment aneurysm hemodynamics in patient-specific CFD simulations to a patient's treatment outcome and suggested candidate thresholds in fluid mechanics variables, such as intra-aneurysmal velocity reduction, that could be predictive of successful treatment. This goal has been elusive, however, and both fundamental research and translational research on large patient cohorts are necessary to obtain conclusive fluid mechanics predictors of aneurysmal treatment outcome.

Despite the vast body of work on the mechanics of FDS-treated intracranial aneurysms, a rigorous parametric characterization of this flow environment, comparing it to the flow in a spherical cavity on the side of a curved pipe (a canonical flow representative of untreated aneurysm fluid mechanics) is missing. This is the primary goal of this paper. In this Part 2, we describe the changes in the flow topologies inside the cavity when it is covered with a porous mesh, comparing them with the flow patterns observed in Part 1, for the unimpeded flow into the cavity on the side of a curved pipe. We perform stereoscopic particle image velocimetry measurements of the flow in the curved pipe (parent vessel), the cavity opening on the side of the pipe (the aneurysmal neck) and inside the cavity (the aneurysm sac).

This experimental study uses parent vessel curvature, κ, parent vessel flowrate, Q, and the frequency of the flow pulsatility, Wo, as dimensional parameters that vary in the physical setup, to explore the influence of the non-dimensional parameters of interest: Dean, Reynolds, and Womersley numbers. The velocity field inside of four geometries with different values of κ, conceived to represent models of idealized *in-vitro* aneurysms, are analyzed at increasing mean Reynolds numbers and under both steady and unsteady forcing.

2. Methods

Briefly, the flow field in four idealized aneurysm models treated with a flow-diverting stent is measured using Stereo-PIV under steady and unsteady flow-conditions. The aneurysm diameter, $D_{aneurysm}$ and parent vessel diameter, D_{PV}, are 7mm and 4mm respectively, and the parent vessel curvature, κ, ranges from $0{:}0.22mm^{-1}$. The flowrates under steady conditions are 100, 200, 300, 400 mL/min equaling parent vessel Reynolds number, Re, values of 120, 240, 360, 480. This provides an effective Dean number range of 0:450: $De = Re\sqrt{\kappa D_{PV}/2}$. For pulsatile flow-conditions, the cycle-averaged flowrate and Re is set to match the same four condtions as the steady cases, and two values of Womersley number, Wo, are investigated: 2.6 & 3.6. Womersley number is defined as $Wo = 0.5D_{PV}\sqrt{2\pi/T\nu}$ where T is the length of the cardiac-cycle and ν is the kinematic viscocity. More details on the experimental setup and measurement methods can be found in Part 1 (Chassagne *et al.* 2021).

A flow-diverting stent is introduced into each aneurysm model by an experienced neurosurgeon who "treats" the physical model with a braided mesh cylinder woven from platinum/tungsten and cobalt-chromium-nickel alloy wires (a flow-diverting stent, 4x20

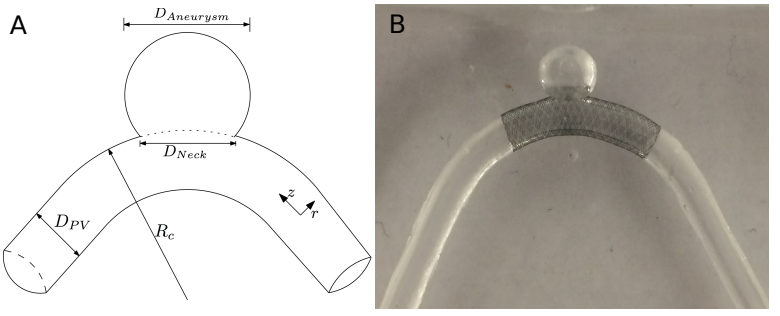

Figure 1: (*a*) Sketch of the idealized cerebral aneurysm with the key geometrical parameters used to define the study. (*b*) Silicone model of a side-wall cerebral aneurysm treated with a clinically-used stent along the parent vessel. The curvature in this case is $0.0625mm^{-1}$

mm PipeLine Embolization devices, Medtronic, Dublin, Ireland) as shown in figure 1(b). The mesh lies along the pipe length, centered on the region where the cavity opens on the pipe wall, covering it completely. These stents are designed for parent vessels with a diameter of 4 mm and can expand, if unimpeded, to a diameter of 4.25 mm. They are 20 mm long and comprised of 48 braided wires, with half spiraling in a clockwise direction, and the other half in a counter-clockwise direction. Each wire has a diameter of 33 μm.

3. Steady Freestream Flow

3.1. *Aneurysm Flow Field Topology*

The contours of velocity magnitude at the aneurysm mid-plane are shown in figure 2 for all parent vessel flow rates and curvatures. Streamlines are used to highlight the direction of the flow inside the aneurysm with flow in the parent vessel (not shown) traveling from right to left. At the lowest De, upper left, the flow expands into the aneurysm at the leading (upstream) edge and exits at the trailing (downstream) edge of the aneurysmal cavity, resulting in counter-clockwise rotation (co-rotating with the parent vessel flow) in the aneurysmal dome. This flow topology is similar to low Reynolds number expansion flow over a cavity, without the existence of corner recirculation eddies (Moffat eddies) due to the quasi-spherical geometry. In the work done by Higdon (1985), high Reynolds number flow inside of a circular cavity with this level of depression was shown to be comprised of a single counter-rotating vortex. The fact that flow in this aneurysm is attached and co-rotates with the parent vessel flow is the result of the FDS slowing down flow inside the cavity, and subsequently acting as a barrier between the viscous dominated aneurysm flow and high inertia of the parent vessel flow.

As the De increases, however, either by increasing parent vessel flowrate (down the rows) or curvature (left to right, across rows), the flow inside the aneurysm begins to separate and two recirculation eddies form. At intermediate De, both clockwise and counter-clockwise rotating eddies exist inside the aneurysm, and the entrance location of flow into the aneurysm shifts downstream. Further increases in De (panels along the bottom and right edge of the 4x4 image matrix) results in a single recirculating vortex with the flow entering the aneurysm at the trailing edge and exiting at the leading edge of the cavity.

In figure 3, the velocity magnitude is shown at the midplane of the parent vessel for all values of Re and κ. The location of peak velocity magnitude can be seen to shift

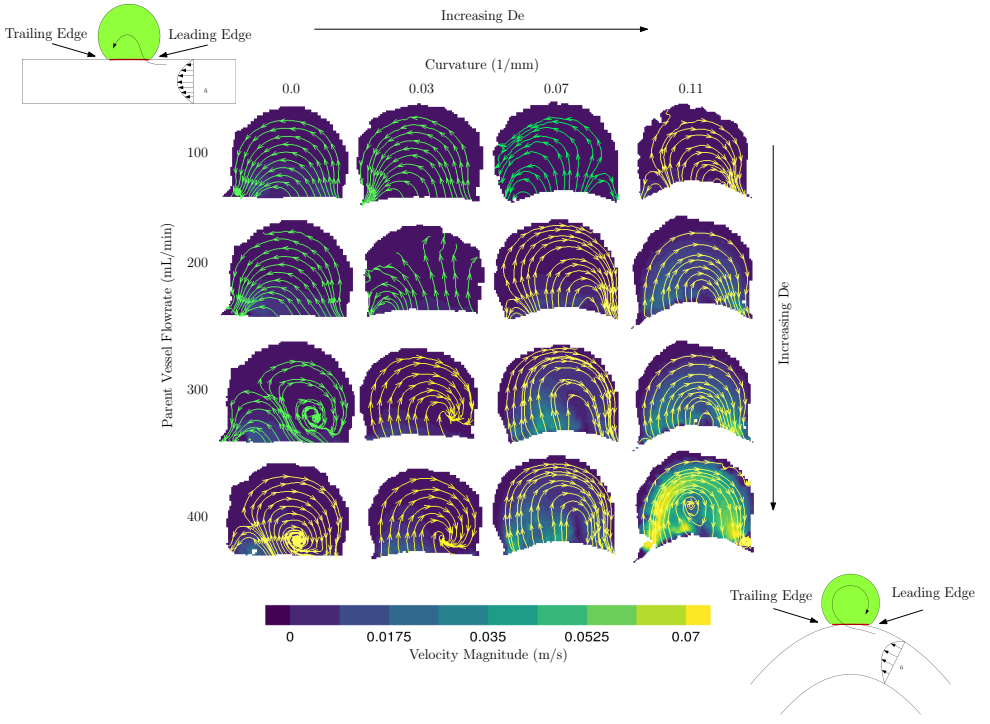

Figure 2: Velocity contours and streamlines at the streamwise mid-plane of the aneurysm sac. Flow inside the parent vessel (not shown) is from right to left. Parent vessel flowrate (or Re) increases with descending rows and parent vessel curvature increases moving left to right in columns. De increases along the diagonal.

towards the outer wall with increasing Dean number (which increases with increasing parent vessel curvature and Reynolds number). The axial velocity profiles, plotted in figure 4(left), are computed by dotting the three dimensional velocity measurements with the vector normal to the extraction line. In the straight aneurysm model, the axial velocity profile is parabolic, as expected at this laminar Reynolds number, and increases in magnitude with flowrate. In the curved models, the axial velocity profile begins to shift towards the outer wall. The construction of the aneurysm models is such that the arc-length of the model shortens with increasing κ. In figure 4(left), the shift in axial velocity towards the outer wall is less pronounced in the model with $\kappa = 0.22mm^{-1}$ than it is for the two other models with smaller curvature. This is because the arc-length from entrance region to measurement plane is shortest for $\kappa = 0.22mm^{-1}$, and the flow is still developing, a phenomenon highlighted in Bovendeerd *et al.* (1987).

In figure 4(right), the details of axial velocity measurements near the outer wall, at the leading edge of the aneurysm, are highlighted. The velocity field is extracted along a line extending from the leading edge of the aneurysm sac, to the centroid of the parent vessel. Each line in the figure is colored by the flow topology inside the aneurysm (clockwise or counterclockwise vortices) for the corresponding flow and curvature conditions. Inspection of the parent vessel flowfield, right at the leading edge, shows that the topology of the flow inside the aneurysm is a function of the streamwise velocity at the aneurysm neck (specifically the shear stress at the cavity leading edge

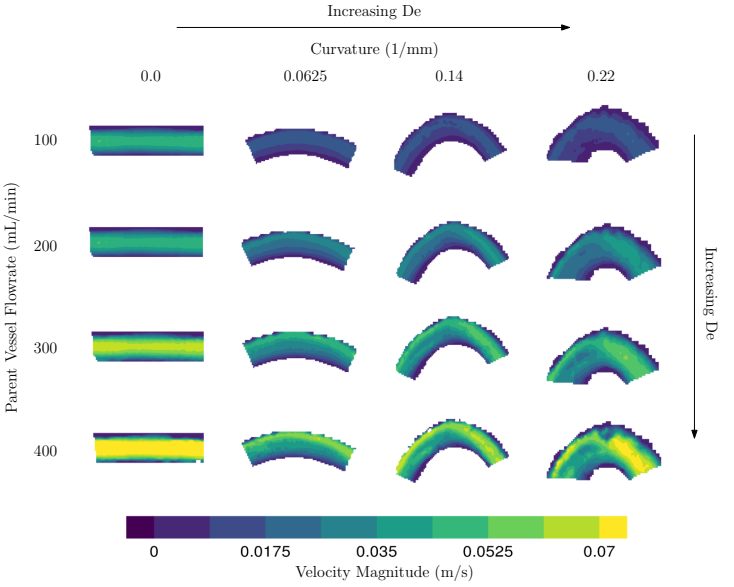

Figure 3: Contours of velocity magnitude (m/s) measured at the mid-plane of the aneurysm parent vessel. Parent vessel flowrate (Re) increases with descending columns and parent vessel curvature increases left to right across rows. De increases along the diagonal.

that determines whether flow detaches or remains attached to the cavity wall), which in the case of curved vessels, is parameterized by De.

The axial velocity profile extracted from conditions that resulted in a single recirculating vortex inside the aneurysm are colored in blue, and those with any counter-clockwise rotation are highlighted in green. A clear separation is seen in the slope of the axial velocity at the leading edge of the aneurysm cavity (the shear at the wall) for the two flow topologies. The critical De, above which flow at the leading edge separates and the sense of rotation inside the aneurysm is entirely opposite the bulk flow direction (clockwise), is ≈ 180.

At a sufficiently low Re, the flow inside the aneurysm remains attached to the wall and travels in the same direction as the bulk flow (upper left corner in figure 2). In the straight model, increasing Re eventually leads to flow separation, recirculation, and a downstream shift in the entrance location of parent vessel flow into the aneurysm. As the curvature of the parent vessel increases, this transition from attached, forward-rotating flow, to fully counter-rotating circulation flow in the aneurysmal sac happens at lower values of parent vessel Re.

3.2. *Aneurysm Velocity Characterization*

The velocity vectors at the neck of the aneurysm are extracted along curves just above the FDS, at each measurement plane. The vectors extracted from the mid-plane are shown in figure 5, colored by the magnitude of the component normal to the aneurysmal neck surface ($\boldsymbol{u} \cdot \boldsymbol{n}$). Again, parent vessel Re increases with descending rows and parent vessel curvature increases with columns from left to right. The direction of the flow entering the aneurysm is highlighted here with non-separated, counter-clockwise rotation occurring at the lowest De (upper left), and separated, clockwise rotation occurring with increasing De (bottom right).

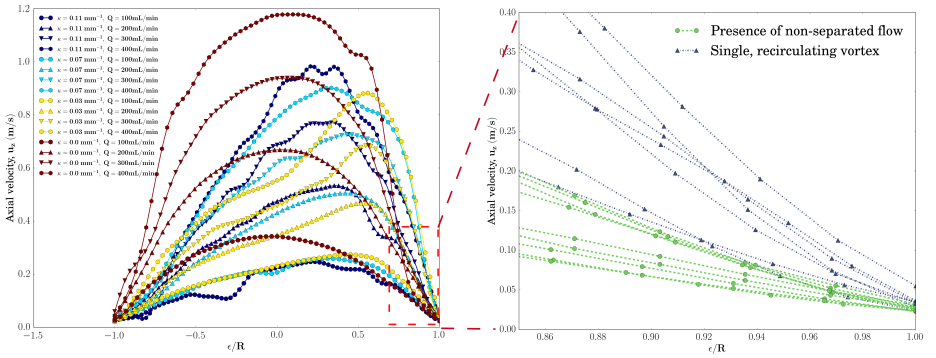

Figure 4: (left) The axial velocity profile extracted from each experimental condition at the mid-plane of the parent vessel. (right) A zoomed in view of the axial velocity profile at the leading edge of the aneurysm neck. Velocity profiles are colored blue if the flow inside the aneurysm has separated and is rotating clock-wise, and green if any counterclockwise rotation exists inside the aneurysm.

Aneurysm inflow velocity, $\bar{u}$, is plotted against flowrate in figure 6a (Part1, eq. 2.1). The average aneurysm inflow velocity increases with increasing parent vessel flowrate and with parent vessel curvature for all models. Figure 6(b) shows the aneurysm inflow Reynolds Number ($Re_{neck} = \bar{u}D_{neck}/\nu$), plotted against parent vessel De. For all models with curvature, the Re_{neck} values collapse onto a single curve, indicating that the amount of flow that enters the cerebral aneurysm sac, treated with FDS, is a function of parent vessel De only. The shift in axial velocity towards the outer wall in a curved vessel is accompanied by secondary vortices transporting fluid along the center-plane from the inner to the outer wall. The magnitude of the outward radial velocity component at the midplane of the parent vessel increases with increasing De and, as a result, the magnitude of flow entering the aneurysm also increases.

In the straight model, the radial velocity component is zero upstream of the aneurysm. At the leading edge, flow expands into the aneurysm, creating a radial velocity component which is a function of axial velocity, aneurysm geometry, and stent porosity. Increases in parent vessel inertia lead to separated flow with the point where the parent vessel flow enters the aneurysmal sac moving downstream (but never reaching the trailing edge). Because the vessel is not curved, there are no increases in parent vessel radial velocity due to secondary vortices, so the increase in aneurysm inflow velocity with parent vessel Re is limited, as seen in figure 5.

In the curved vessels, the aneurysm inflow velocity is heavily influenced by the radial velocity generated by the pressure gradient associated with the sudden expansion, and the secondary (Dean's) vortices in the parent vessel created by the curvature, and subsequent inertial instability. Since aneurysm inflow velocity is approximately equal for all cases at the lowest parent vessel Re, the radial velocity that arises due to secondary vortices is small compared to that due to the pressure gradient at the expansion, for the lowest value of parent vessel Re. However, with increasing parent vessel inertia, the aneurysm inflow velocity in all curved models rapidly becomes larger than that of the straight vessel, indicating that the radial velocity in the aneurysm generated by the curvature-induced flow in the parent vessel becomes the driving component in aneurysm inflow velocity at higher De.

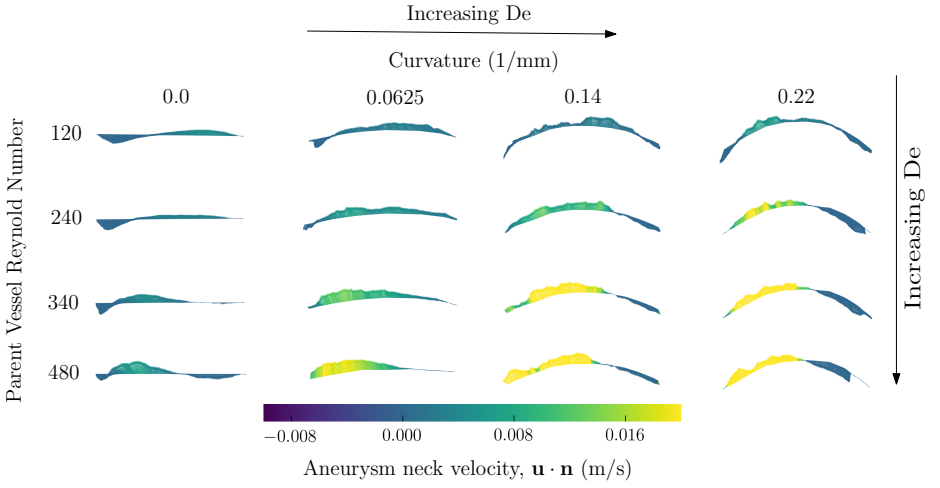

Figure 5: Velocity vectors extracted from the aneurysm neck at the mid-plane. Vectors are colored by the magnitude of $\mathbf{u} \cdot \mathbf{n}$

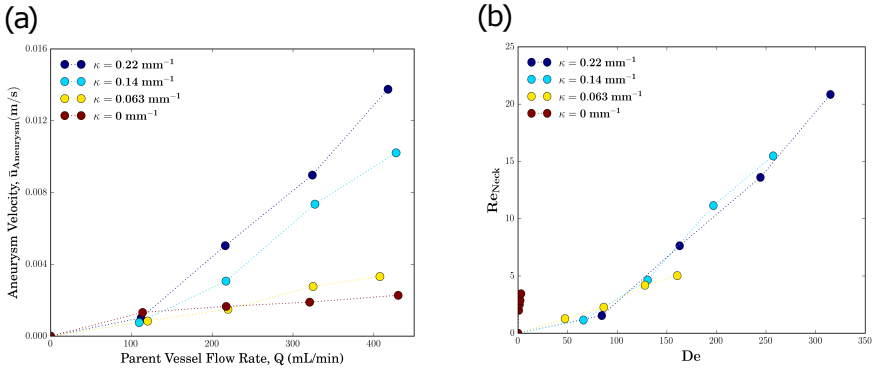

Figure 6: The average aneurysm inflow velocity for each value of parent vessel curvature and flowrate shown in dimensional (a) and non-dimensional units (b)

4. Unsteady Freestream Flow

4.1. *Flow Structure Across the Cardiac Cycle*

In figure 7, the aneurysm flow-field is plotted at 5 instants during the cardiac cycle for the condition κ=0.0625 mm^{-1}, $Re = 320$, and $Wo = 2.6$. In each snapshot of this representative case, streamlines at the aneurysm mid-plane are overlaid on contours of the y-component of velocity (component of velocity entering and exiting the aneurysm), $u_{aneurysm}$. At the beginning of the cardiac cycle (A), as the parent vessel flow starts to accelerate, the flow entering the aneurysm remains attached to the leading edge of the aneurysm cavity. Towards the end of the accelerating phase (B), the flow remains attached, yet the primary vortex in the aneurysm begins to shift towards the distal edge of the aneurysm, and the flow entering the aneurysm at the leading edge no longer rotates with the primary aneurysm vortex. Right at peak systole (C), the aneurysm flow separates at the leading edge. This counter-rotating vortex then continues to grow until it encompasses the entire aneurysm dome during the deceleration phase (D). Towards the end of the cardiac cycle (E), the counter-rotating vortex begins to break down and

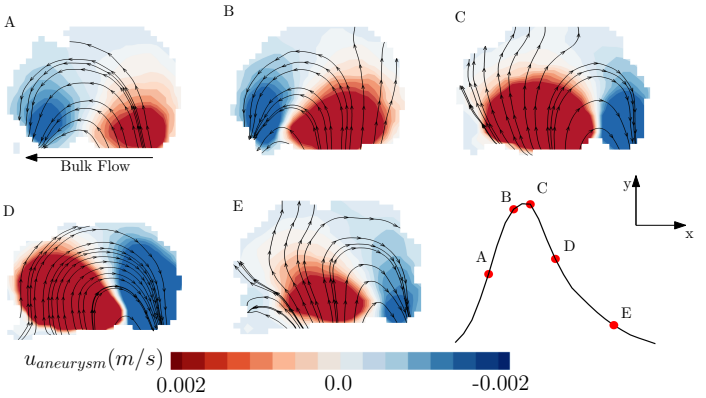

Figure 7: Velocity contours and streamlines at the aneurysm mid-plane for the condition: $\kappa = 0.0625\ mm^{-1}$, $Re = 320$, and $Wo = 2.6$ at 5 locations in the cardiac cycle. Velocity contours are of the vertical componant of velocity, $u_{aneurysm}$

flow at the distal edge of the aneurysm once again rotates with the primary direction of the parent vessel flow.

The structure of the flow at the leading edge of the aneurysm is primarily controlled by two pressure gradients, both functions of the flowrate entering the aneurysm, $Q(t)$. As flow expands into the aneurysm, an adverse pressure gradient develops at the leading edge of the aneurysm wall which is proportional to $Q(t)^2$. A second pressure gradient exists due to the acceleration of the fluid which is proportional to $\partial Q(t)/\partial t$. As soon as flow begins entering the aneurysm, the adverse pressure gradient begins to grow. At the beginning of the cardiac cycle, however, when $\partial Q(t)/\partial t$ is positive, the acceleration-based gradient is also positive and acts to keep the flow attached to the leading edge. As $Q(t)$ increases, however, and the cardiac cycle moves through systole, $\partial Q(t)/\partial t$ decreases while the expansion-based pressure gradient increases in magnitude. Eventually, the magnitude of the expansion-based pressure gradient becomes larger than the acceleration-based gradient, and flow at the leading edge begins to separate. Throughout diastole, with the acceleration-based gradient becoming negative, the separated aneurysm vortex continues to grow until it fills the entire aneurysm cavity.

4.2. *Inertial Effects (Dean and Reynolds Number)*

In figure 8, velocity contours and streamlines are plotted for the same aneurysm model ($\kappa = 0.22mm^{-1}$) at increasing values of parent vessel Re. Each panel shows the flowfield at the same instant in the cardiac cycle. At the lowest values of parent vessel Re, the flow remains completely attached to the aneurysm wall, rotating in the direction of the bulk-flow. As the Re increases, the flow topology shifts, from attached forward-rotating to separated counter-rotating flow at the same point in the cardiac cycle. In other words, the flow begins to separate at an earlier point in time as the Re is increased.

This is further visualized in figure 9, where the the area-averaged vorticity, or aneurysm circulation, $\Gamma(t)$ is plotted over the cardiac cycle, normalized by the circulation calculated at peak systole, Γ_s, for the same conditions shown in figure 8. The dashed vertical line indicates the snap-shot in time where the four panels in figure 8 are shown. At the lowest value of parent vessel Re, the aneurysm circulation becomes negative at the beginning of the cardiac cycle and eventually transitions to positive (indicating primarily separated flow) about $1/5^{th}$ of the way through the cardiac cycle. As the Re is increased, this

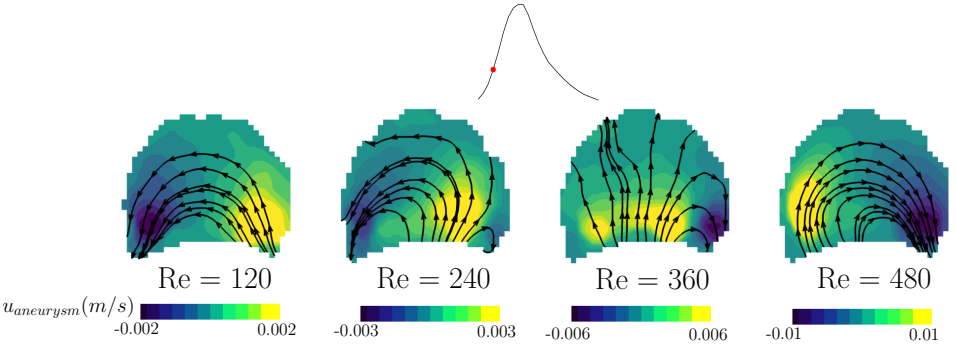

Figure 8: Velocity contours and streamlines at the aneurysm mid plane for the condition, $\kappa = 0.22mm^{-1}$, $Wo = 2.6$. Each plane highlights a snap-shot from the same location in the cardiac-cycle (half way through acceleration) for increasing values (left to right) of cycle-averaged Reynolds Number. Velocity contours are of the vertical componant of velocity, $u_{aneurysm}$

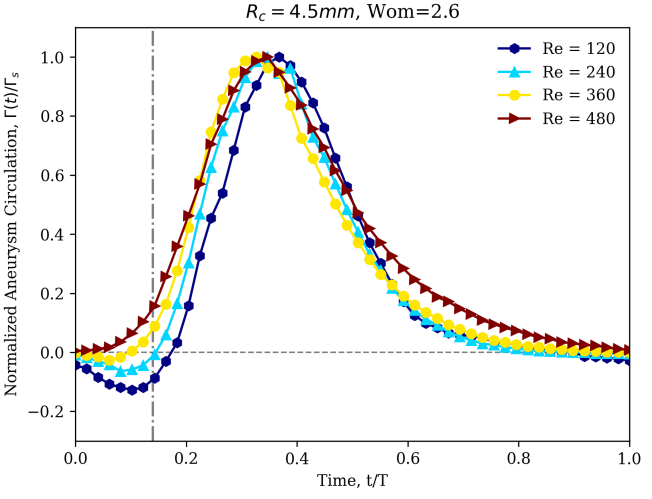

Figure 9: Aneurysm averaged vorticity plotted across a single cardiac cycle for: $\kappa = 0.22\ mm^{-1}$, $Wo = 2.6$. Aneurysm vorticity is normalized by peak systolic vorticity.

transition from attached to separated flow with the average vorticity becoming positive, occurs at an earlier point in the cardiac cycle. The time it takes for separation to occur, from the beginning of the cardiac cycle, is defined as the separation time: T_s.

Increasing the parent vessel Reynolds number results in an increase of flow entering the aneurysm (6A). As the expansion-based pressure gradient is proportional to $Q(t)^2$, and the acceleration-based pressure gradient is only proportional to $\partial Q(t)/\partial t$, increasing the *Re* results in faster growing and dominating adverse pressure gradients. Thus, for the same geometry, an increase in *Re* results in separation that occurs earlier in the cardiac cycle.

The transition from attached to separated flow during the cardaic cycle has been previously documented in studies on untreated (Asgharzadeh & Borazjani 2016) and

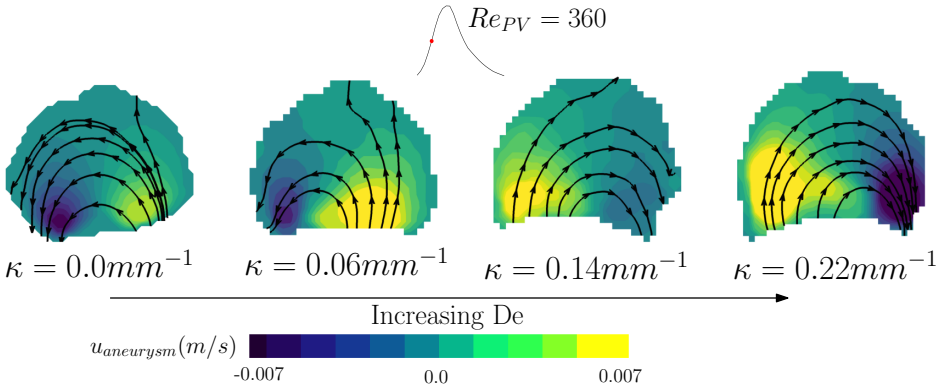

Figure 10: Velocity contours and streamlines at the aneurysm mid-plane for the condition, $Re = 360$, $Wo = 2.6$. Each plane highlights a snapshot from the same instant in the cardiac-cycle (half way through acceleration) for increasing values (left to right) of curvature, and thus, increasing De. Velocity contours are of the vertical componant of velocity, $u_{aneurysm}$

FDS treated aneurysms (Lieber *et al.* 2002), but only in straight idealized aneurysms. The dependence of the time of separation on inertia and the topology of the flow over a spherical cavity was highlighted by Sobey (1980), where an increase in freestream Reynolds number results in lower separation times. Here, we extend upon this work and also explore the effect of freestream geometry by varying curvature and including the De in the analysis.

In figure 10, velocity contours and streamlines are plotted for four values of parent vessel curvature, at the same value of Re (increasing De). All four panels represent the same instant in the cardiac cycle: half way through the acceleration phase. As the De increases, the structure of the flow, at the same instant of time, evolves: the flow remains attached at the lowest value of De, while it is fully separated at the highest value of De.

This is the same behavior seen in figure 8. At the same instant in the cardiac cycle, vessels with larger curvature, or De, will have more flow entering the aneurysm cavity (6B). With the Re and waveform fixed for all cases in figure 10, the magnitude of the acceleration gradient is approximately equal at the same moment in time. The adverse pressure gradient, proportional to the flowrate entering the aneurysm, however, will have a larger value at the same instant in time, resulting in flow separation at an earlier time in the cardiac cycle.

In figure 8, by increasing the Re while maintaining the vessel curvature, the De is also increased. This begs the question of whether flow separation is predominately a Re or De effect. In figure 11 each panel (a and b) contains streamlines and velocity contours plotted at the same De, but different Re, at the same instant in the cardiac cycle. De is matched at different Re by selecting vessels with different curvature. At both values of De, the flow patterns are nearly identical despite having different values of parent vessel Re. This suggests that the flow topology inside the aneurysm and the separation time, is truly a function of De only.

4.3. *Transient Inertial Effects (Womersley Number)*

In figure 12(a), the separation time is plotted against parent vessel De for both values of Wo. The separation time is shown to decrease with increasing De, and the functional decay of separation time with De is the same for both values of Wo: at a given De,

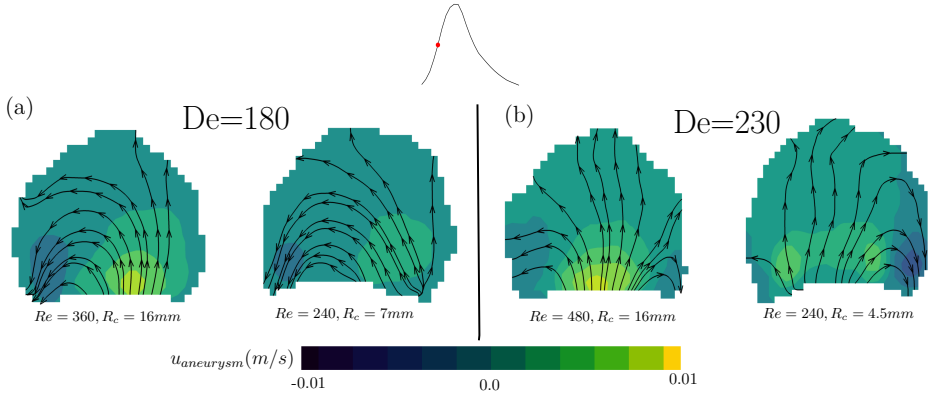

Figure 11: Velocity contours and streamlines for two models with approximately matching De: $De \approx 180$ (a) and $De \approx 230$ (b). In each panel (a and b) models are selected with different Re and R_c, but matching De. Velocity contours are of the vertical componant of velocity, $u_{aneurysm}$

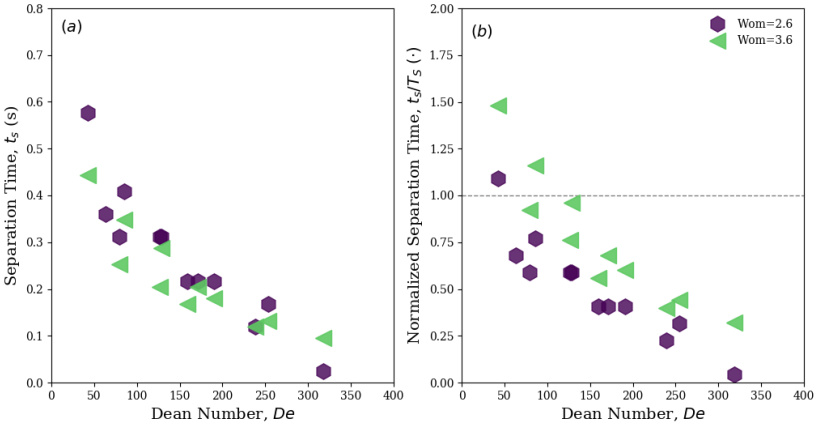

Figure 12: Separation time (a) plotted against Dean number and separation time normalized by peak systole (T_s) (b) for all cases.

separation occurs at the same physical time in the cardiac cycle, regardless of the flow pulsatility (for the range investigated in this paper). Separation time is again plotted against De in figure 12(b) but normalized by the time it takes to reach peak systole, T_s. The vertical dashed line in figure 12(b) represents the transition in the cardiac cycle between the systolic and diastolic phase of the cardiac cycle. For a given De, increasing the Wo causes separation to occur at a later relative phase in the cardiac cycle. By looking at the intersection of the data points and the line $t_s/T_s = 1$, we can estimate a critical De for which separation occurs in the accelerating or decelerating phase of the cardiac cycle. As an increasing Wo pushes separation into a later phase of the cardiac cycle, the critical De for separation occurring during systole also increases: it takes the values ≈ 75 and 150 for $Wo = 2.6$ and 3.6 respectively.

To investigate the effect of Wo, non-dimensional parent vessel flowrate, $Q(t)/Q_{sys}(t)$, and acceleration $\partial Q(t)/\partial t$, are plotted against time, both in dimensional form and non-

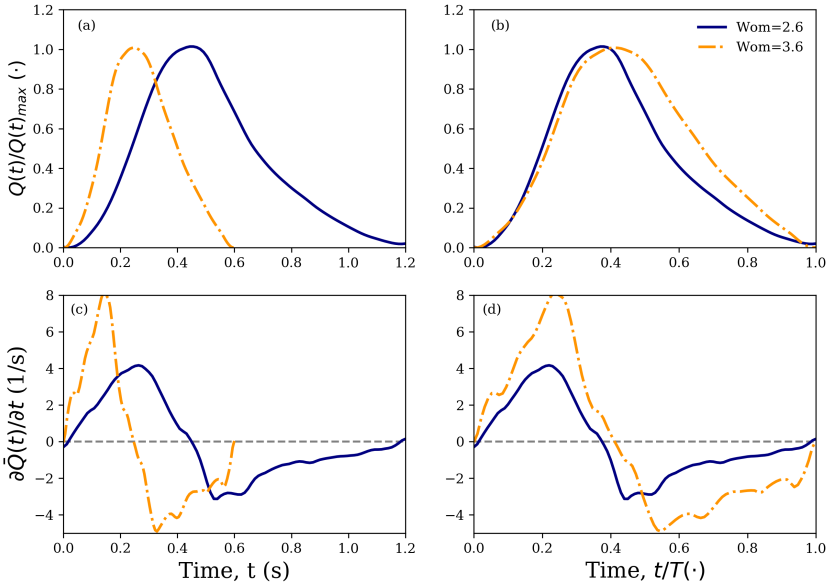

Figure 13: Parent vessel flowrate non-dimensionalized by systolic flowrate, $\bar{Q}$ and plotted against time (a) and time non-dimensionalized by cardiac cycle length (b). Time derivative of flowrate (acceleration) plotted against dimensional (c) and non-dimensional time (d)

dimensionalized by the length of the cardiac cycle, for Re=200 and both values of Wo. The occurrence of separation is primarily dependent on the interplay between the two pressure gradients which are proportional to these curves. Increasing the Womersely number shortens the cardiac cycle which, at the beginning of the cardiac cycle, increases both the magnitude of the instantaneous flowrate and of the acceleration as seen in sub-figures (a) and (c). Separation occurs at the same time for both values of Wo (at a given De) because the ratio between the expansion-based and acceleration-based pressure gradients remains the same.

In figures 13 (b) and (d), the same curves are plotted against time, non-dimensionalized by the cardiac cycle period. In the acceleration phase, it can be seen that the magnitude of flowrate is nearly identical for both values of Wo. However, the magnitude of the acceleration is larger for the larger Wo case. This suggests that flows with a higher Wo are able to remain attached for longer and separate at a later instant in the cardiac cycle, as is seen in 12(b). As flow attachment is maintained by this acceleration-based pressure gradient, an increase in Wo will also result in a higher critical De for separation to occur in the acceleration phase.

In the work by Sobey (1980), it was shown that separation time depends on both Reynolds number and the frequency of bulk flow pulsatility or Strouhal Number (St). An increase in St was shown to increase separation time (non-dimensionalized by period length) for the same value of Re. The same trend is shown here except that Wo replaces St and De replaces Re as we have added the influence of curvature. Sobey (1980) also discusses a critical Re below which separation occurs only in the deceleration phase of the the pulsatile flow phase. This critical separation behavior is shown to be a function

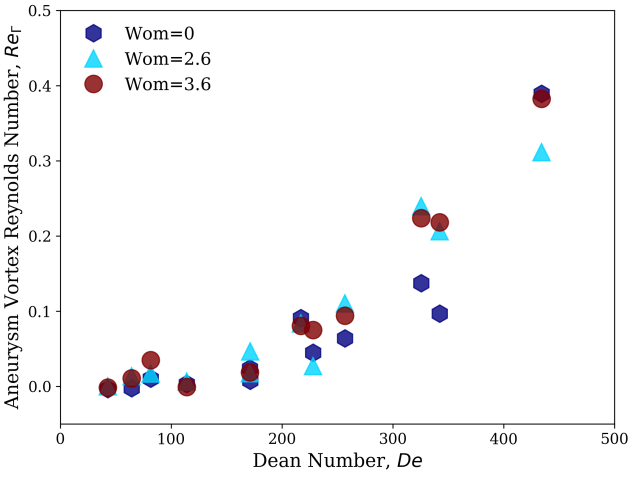

Figure 14: Aneurysm vortex Reynolds number as a function of Dean number for all values of Womersley number

of St and, above a St of 0.1, flow is only able to separate in the deceleration phase of the cycle, regardless of Re. The St of the flow waveforms studied here are below 0.1 ($St = 0.007 - 0.03$), but the trend in figure 12(b) suggests that further increases in Wo would eventually result in a condition where separation only occurs in the deceleration phase of the cardiac cycle.

The effect of unsteady flow on Eulerian metrics is investigated by calculating the Reynolds number based on the circulation inside the aneurysmal sac, $Re_\Gamma = \Gamma_{Aneurysm}/\nu$. In figure 14, the aneurysm vortex Reynolds number, Re_Γ, is plotted against Dean Number for all values of Womersley number investigated here, including steady flow ($Wo = 0$). For pulsatile cases, $Wo = 2.6$ & 3.6, the circulation inside the aneurysm is phase-averaged over the cardiac cycle. First, it can be seen that the strength of the vorticity inside the aneurysm is a function of Dean number, with the strength of vorticity increasing with increasing Dean number. The cycle-averaged vortex strength for both values of Wo is also shown to be equivalent for a given De, with the phase-averaged values for pulsatile cases equaling the corresponding steady flow values ($Wo = 0$). This suggests that pulsatility has little influence on the phase-averaged values of vortex strength inside the aneurysm for the parameter range studied here.

In a numerical analysis, Asgharzadeh & Borazjani (2016) investigated the effect of Reynolds and Womersley number on the vortex structure in untreated idealized and patient-specific aneurysm models. It was shown that Womerlsey number has little effect on the structure and characteristics of the primary aneurysm vortex, but that it did effect the location of the vortex at different instances of the cardiac cycle. This is similar to the findings presented here where the primary structure of the aneurysm flow-field and cycle-averaged metrics are not impacted by the Wo (in the range studied here) but the temporal evolution of the aneurysm vortex during the cardiac cycle is impacted.

Due to the flow-diverting stent, the aneurysm vortex Reynolds number is small ($Re_\Gamma < 1$). Thus, the viscous- dominated aneurysm flow behaves similar to a linear Stokes flow where cycle-averaged metrics for pulsatile flows are equal to the steady flow values with the same mean freestream flow. At higher values of aneurysm Re, we'd expect that the

curves shown in figure 14 would begin to diverge but, for the parameter range studied here, that is representative of the physiological values in FDS-treated cerebral aneurysms, the Womersley number is shown to have little influence on the characteristics of the flow, and De is the driving non-dimensional parameter (centrifugal inertia in the parent vessel injecting flow into the aneurysm cavity is the main mechanism).

5. Comparison of Fluid Mechanics inside Untreated (Part 1) and FDS-Treated (Part 2) Aneurysms

5.1. *Steady Freestream Flow*

The primary function of FDS-treatment is to restrict flow into the aneurysmal cavity and create an environment inside the aneurysmal sac that promotes the growth of a stable thrombus, isolating the aneurysmal wall from mechanical stresses associated with the flow of blood and, thus, reducing the risk of rupture. In figure 15, the Reynolds number computed from the average inflow velocity measured at the neck of the aneurysm, Re_{neck}, is plotted as a function of parent vessel Dean number for treated and untreated cases under steady freestream flow conditions. Across the entire range of Dean numbers studied, the magnitude of velocity entering the aneurysm is approximately an order of magnitude lower in the treated than in the untreated cases. Additionally, the degree or magnitude of flow reduction is nearly constant across all Dean numbers, as is evident in figure 15.

This significant reduction in aneurysmal flow results in markedly different flow topologies in the aneurysmal cavity. From figure 3 in Part 1, the flow is shown to be separated at the cavity leading edge, and rotating in the direction opposite the freestream flow for all vessels (with different curvatures) and all values of Reynolds number. However, in figure 3 in Part 2, the flowfield remains attached to the aneurysmal wall at low Dean numbers and begins to separate forming a counter-rotating vortex as the Dean number increases. A comparison between three treated (bottom) and untreated (top) flowfields for the same conditions is shown in figure 16. The first two cases are for straight vessels ($\kappa = 0.0mm^{-1}$) at Reynold numbers of 120 and 360. For both untreated cases, the flow is fully separated with a single counter-rotating vortex inside the cavity. For the treated model, the flow remains fully attached at the lowest Reynolds number, but begins to separate at the higher Reynolds number (in the second panel). The third panel shows the flowfields for the higher curvature vessel ($\kappa = 0.14mm^{-1}$) and a Reynolds number of 140. At this higher Dean number, both flowfields exhibit the same topology, but the magnitude of velocity and circulation is much higher in the untreated case.

Separation in the aneurysm cavity occurs when the adverse pressure gradient that results as flow expands into the aneurysm is greater than the inertia in the parent vessel near the wall, at the aneurysmal leading edge. For the flow to remain attached at the leading edge, the flow near the aneurysmal wall must be sufficiently slow to enable viscous forces to dominate over inertia. This condition is only achieved, in the flow-regimes relevant for cerebral aneurysm, when a FDS is placed across the neck of the aneurysm and flow entering the sac is significantly restricted.

5.2. *Unsteady Flow*

For unsteady freestream flow conditions, the trends are similar to the steady freestream conditions: the magnitude of flow entering the aneurysm is decreased for treated cases resulting in large differences in the topology of the flow, that develop across the duration of a cardiac cycle. In part 1, the flow in the aneurysm was shown to be counter-rotating for

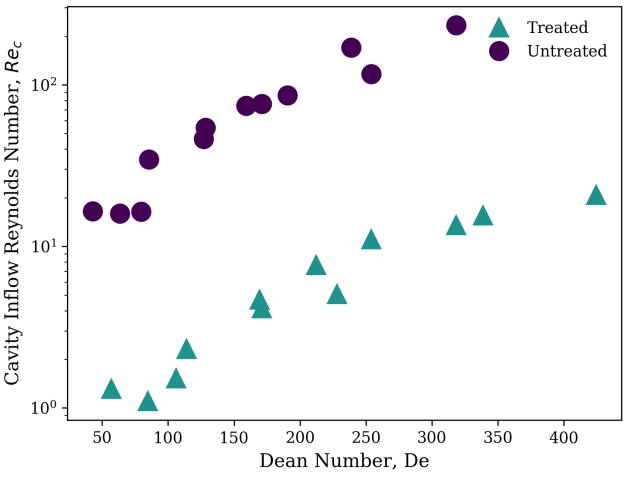

Figure 15: Cavity inflow Reynolds number as a function of Dean Number for treated and untreated models

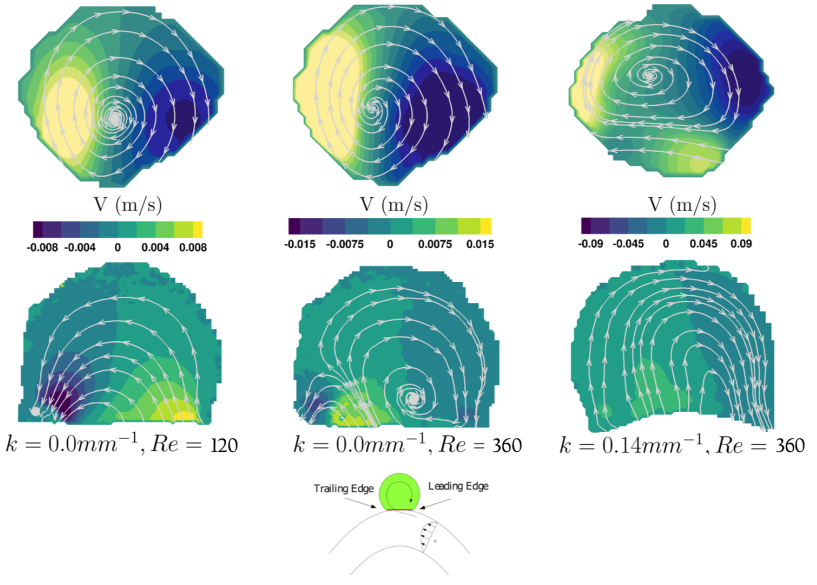

Figure 16: Streamlines plotted at the aneurysm mid-plane for untreated (top) and treated (bottom) cases

the entirety of the cardiac cycle, for all conditions. The flow vorticity inside the aneurysm increases and decreases throughout the cardiac cycle but the primary structure of the aneurysm flow remains unchanged with a single counter-rotating vortex persisting in the aneurysm cavity. In part 2, it is shown that at low values of Dean number the flow in the aneurysm cavity is attached at the beginning of the cardiac cycle, and separates only during the deceleration phase of the cardiac cycle. At higher values of Dean number, the instant at which the flow becomes separated and counter-rotates shifts earlier towards

the start of the systolic phase, but all cases start the cardiac cycle in the co-rotating, attached flow topology.

In figure 17 (left), the circulation inside the aneurysm is normalized by peak circulation and plotted throughout the cardiac cycle for three conditions, for both treated and untreated cases. For all of the treated vessels, at the start of the cardiac cycle the vorticity is negative indicating attached flow. Circulation becomes positive, indicating primarily separated flow inside the aneurysm, during the first third of the cardiac cycle. As the Dean number increases, this transition point, from co-rotating to counter-rotating flow, happens earlier in the cardiac cycle (figure 12). For the untreated cases, the circulation is positive (separated flow) throughout the entire cardiac cycle and the baseline magnitude of circulation as a percentage of peak circulation, increases with increasing Dean number. The higher the Dean number, the more momentum is maintained from the previous acceleration phase, resulting in higher values of circulation at the start of a new cardiac cycle.

In figure 17 (right), the peak circulation is plotted as a function of Dean number for treated and untreated cases at $Wo = 2.6$ and 3.6. For both treated and untreated, the value of peak circulation increases with increasing Dean number. Again, there exists an approximate 10-fold reduction in the magnitude of peak circulation between the untreated and treated cases. The exception is the circulation at the lowest values of Dean number, where there is a 1000-fold reduction in circulation for the treated case, compared to the untreated. For treated cases, the flow starts the cardiac cycle attached to the wall and separates during the deceleration phase. This late transition to counter-rotating flow delays the development of a counter-rotating aneurysm vortex, and prevents the vortex from reaching a significant strength, as it does for conditions that start the cardiac cycle in the separated flow topology. While the effect of Wo on values of peak circulation is negligible for the untreated cases and the treated cases with higher De, there is larger variation in peak circulation between $Wo = 2.6$ and $Wo = 3.6$ at low values of De for treated cases. This subset of cases, treated with small De, is most significantly affected by flow-switching (from attached to separated flow). Thus, for a given De, the vorticity in cases with a higher Wo, or shorter cardiac cycle, has less time to develop and tends to have a smaller peak circulation value than cases with a smaller Wo.

6. Conclusions

In this study, the fluid mechanics of cerebral aneurysms are characterized in detail, by varying the three key non-dimensional parameters: Re, De, and Wo. FDS treatment restricts flow into the aneurysm, resulting in significantly lower velocities inside the aneurysm than in the parent vessel. As a result, the flow inside the aneurysm is dominated by viscous effects and behaves similar to a linear Stokes flow in a side cavity, despite the Re in the parent vessel being in the range of 100-600.

Under steady freestream conditions, the flow topology in the aneurysm is shown to be a function of De only. At low values of De, the flow enters the aneurysm at the leading edge and remains attached to the aneurysm wall with a single vortex inside the aneurysm that rotates with the direction of the freestream flow - a flow characteristic that is found in low Re flow over cavities (Higdon (1985)). As the De increases, secondary flow instabilities develop in the parent vessel and higher flowrate enters the aneurysm cavity, increasing the magnitude of the adverse pressure gradient at the leading edge of the aneurysm. Eventually this adverse pressure gradient overcomes the parent vessel inertia near the wall, and the flow at the leading edge of the aneurysm separates. This forms a recirculating vortex that competes with the co-rotating vortex induced by

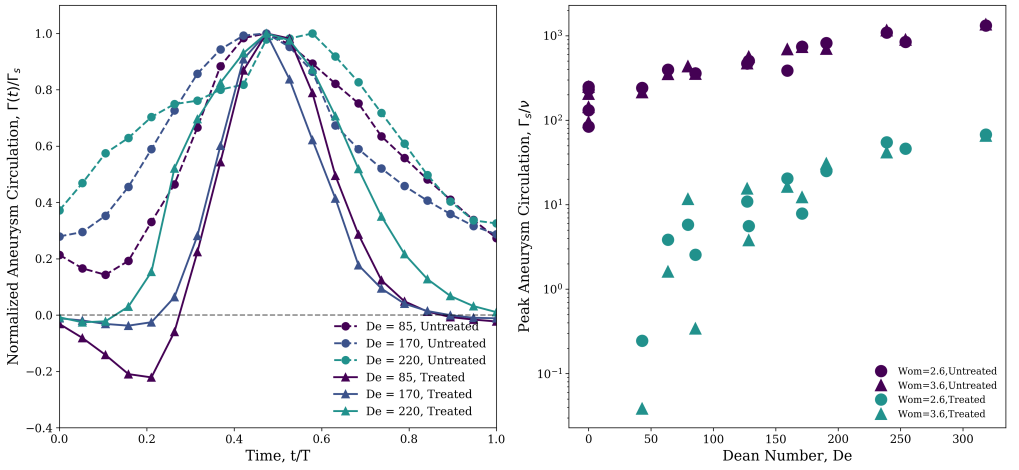

Figure 17: Aneurysm circulation normalized by peak circulation (systole) plotted throughout the cardiac cycle for three representative models. $Wo = 2.6$ for all models (left). The magnitude of peak circulation plotted as a function of Dean number for treated and untreated model at Wo= 2.6 and 3.6. (right)

viscous flow and grows with increasing De until a single counter-rotating vortex exists inside the aneurysm. The transition between these two flow topologies, from attached to recirculating, are shown to depend on the slope of the axial velocity at the leading edge of the aneurysm neck, which scales with De.

The aneurysm flow topology follows a similar pattern under pulsatile freestream conditions, except that the evolution from attached to separated flow occurs over the course of a single cardiac cycle. At the beginning of the cardiac cycle, with the parent vessel De at its lowest, the flow remains fully attached to the aneurysmal cavity for all cases studied, and rotates with the direction of the freestream flow. As the flow accelerates, and the cardiac cycle moves closer to peak systole, the flow at the leading edge begins to separate and the recirculation vortex that is formed continues to grow throughout the the cardiac cycle until it encompasses the entire aneurysm cavity. The instant in the cardiac cycle at which the aneurysm flow separates is shown to be a function of parent vessel Wo and phase-average De. All values of phase-average De studied here, which encompass the relevant hemodynamics range for the cerebral circulation, resulted in separated flow in the untreated cases. An increase in phase-average De is shown to reduce the separation time, pushing it closer to the start of the cardiac cycle. For a given Wo, a critical De exists above which flow separates in the accelerating or systolic phase of the cardiac cycle. Increasing the Wo is shown to delay the separation time, pushing it closer to diastole for a given De. Thus, the critical De required for separation to occur before peak systole, also increases with Wo.

The aneurysm inflow velocity and circulation are shown to increase with increasing De. The magnitude of the flowrate into the aneurysmal sac depends on the parent vessel radial velocity and on the resistance, or porosity, of the stent. In Dean flows, the radial velocity at the center of the vessel increases with increasing De due to the radial pressure gradient and inertial instability. The Re inside the aneurysm is low ($Re < 1$) and as a result, Wo is found to have minimal effect on time-average aneurysm circulation: mean values from pulsatile flow conditions are almost identical to those for the equivalent steady freestream conditions. Differences in peak circulation between the two pulsatile Wo cases are found

only in the treated models, and then only at the lowest values of De, corresponding exactly to the narrow parameter range significantly impacted by flow-switching.

Upon comparing the hemodynamics of the treated (Part 2) and untreated (Part 1) aneurysms, a dramatic difference is characterized fully for the first time. The addition of flow-diverting stents is shown to reduce the magnitudes of the flowrate entering the aneurysm and of the peak vorticity by an order of magnitude. The hydraulic resistance associated with the stent drops the aneurysm Reynolds number into a region where the fluid mechanics are viscous-dominated, resulting in the interesting change in flow topologies described.

6.1. *Clinical Implications*

Flow-diverting stents are designed to induce the formation of a stable aneurysm thrombus by redirecting blood flow away from the aneurysm, thus reducing mechanical stresses inside the aneurysm sac and mitigating the risk of rupture (Lieber *et al.* 1997; Rajah *et al.* 2017). While the exact bio-mechanical mechanisms that result in a stable thrombus inside the aneurysm remain unknown, the process is believed to follow a similar pattern to physiological clotting - platelet activation, aggregation, and fibrin clot stabilization/maturation (Ngoepe *et al.* 2018). Crucial to this process is the creation of a hemodynamic environment inside the aneurysm which enables platelet aggregation - flow stasis and increased platelet residence time (Hathcock 2006; Tomaiuolo *et al.* 2017; Rajah *et al.* 2017).

Multiple *in-vitro* (Lieber *et al.* 1997; Babiker *et al.* 2012) and *in-silico* (Damiano *et al.* 2015) studies have demonstrated the effectiveness of flow-diverting stents at restricting the amount of blood-flow that enters the aneurysmal sac. Image-based computational studies have linked the post-treatment hemodynamics environment to treatment outcomes, suggesting that a threshold of reduction of stresses or flow velocities inside the aneurysm exists and must be surpassed for successful aneurysm embolization to occur (Mut *et al.* 2015; Kulcsár *et al.* 2012; Paliwal *et al.* 2017). Most recently an *in-vivo* study using 4D MRI (Su *et al.* 2020) and an image based CFD study (Chen *et al.* 2019) separately linked FDS treatment failure with the existence of a strong inflow jet into the aneurysm sac.

The results presented in this study show that the parent vessel De has a significant impact on the amount of flow entering an aneurysm, both before and after being treated with an FDS. As seen in figures 6 (A) and 14, an increase in either parent vessel flowrate or curvature causes an increase in aneurysm flow velocity and circulation. When comparing the highest curvature vessel to the straight vessel, the increase in aneurysm velocity is almost 8-fold, every other parameter being held constant. The increased hydraulic resistance of the flow-diverting stent used here results in approximately an order of magnitude reduction of aneurysm cavity Reynolds number and peak circulation (figures 15 & 17 (b)). However, we show here that the magnitude of these values increases with De for both treated and untreated cases, and at a De of ≈ 400, the amount of flow entering the aneurysm and the cavity circulation for the treated case are equal to those values for the untreated case at the lowest De (≈ 50). In other words, the flow entering an untreated aneurysm on a straight or slightly curved vessel, is equal to that of an aneurysm located on a vessel of high-curvature that is treated with an FDS. Thus, increases in parent vessel De may significantly compromise the ability of FDS treatment to achieve the necessary reduction in flowrate, velocity and circulation, and the associated necessary increase in residence time inside the aneurysmal sac for successful aneurysm embolization.

Previous studies have shown the influence of parent vessel geometry (Imai *et al.* 2008; Kim *et al.* 2008; Augsburger *et al.* 2009) and flowrate (Lieber *et al.* 2002; Morales *et al.*

2016) on aneurysm hemodynamics, and that increased vessel curvature or parent vessel Reynolds number reduce the efficacy of FDS treatment. In a computational study, Imai *et al.* (2008) investigated the effect of parent vessel geometry on the inflow into untreated sidewall aneurysms by simulating steady flow through arterial bends of different shape. These results showed that the development of secondary flows, established by proximal arterial geometry, are the driving mechanism for aneurysm inflow rate, supporting the importance of De on aneurysm hemodynamics. Kim *et al.* (2008) conducted PIV analysis of sidewall aneurysm models treated with two different flow-diverting stents with increasing values of parent vessel curvature. Using a constant steady inflow condition, it was shown that the ability of flow-diverting stents to reduce aneurysm inflow rate and increase flow-stasis was significantly diminished when placed in vessels with high curvature. The reduction of efficacy in models with high-curvature is attributed to increasing inertia-driven flow. In a similar experimental study, Augsburger *et al.* (2009) compared the PIV flow-field in two sidewall aneurysms: one on a straight vessel and the other on a vessel with high curvature. Subjected to the same pulsatile inflow condition, it was shown that velocity and vorticity values were generally 2 - 3 times higher in the high-curvature model than in the straight model. Lieber *et al.* (2002) measured the flow-field in a sidewall aneurysm located on a straight vessel under increasing inflow rates. Similar to the results presented here, the addition of an FDS caused an order of magnitude reduction in mean circulation. The direction of the flow in the stented cases was additionally shown to be primarily opposite that of the unstented case, in agreement with results presented here for a certain range of the parameter range (but not for other cases), as shown in figure 16. In a computational study, Morales *et al.* (2016) investigated the effect of inlet flowrate on 25 patient-specific models, and found that across all models, stent performance diminished with increasing inlet flowrate or parent vessel Re. The combination of the above studies produces a mosaic of evidence that parent vessel geometry (κ) and flow conditions (Re, pulsatility) significantly impact the degree to which flow diversion is successful. The results presented in this manuscript fully describe this behavior across the entire 3-parameter space, complimenting the earlier evidence produced by those seminal studies, showing that the effect of flow and geometry in hemodynamics, which in principle depends on three independent non dimensional numbers that characterize inertia, can be understood through a single non-dimensional number: De.

There are several practical limitations to this study, which limit the applicability of this work directly to clinical problems. A single type of FDS was investigated, and always on vessels of constant diameter, while in clinical practice, both the stent design (Lieber *et al.* 2002; Wang *et al.* 2016) and the ratio of vessel diameter to intended deployment diameter (Makoyeva *et al.* 2013) impact the stent porosity and subsequent degree of flow-diversion. Additionally, the aneurysms investigated all have the same geometry: spherical, sidewall aneurysms located on a single bend or straight vessel. In reality, aneurysm morphology, proximal arterial geometry, and the aneurysm location will impact the aneurysm hemodynamics. Previous studies have shown that size and shape of aneurysms has minimal effect on inflow patterns, but that the location of the aneurysm in relation to the secondary flows that develop due to the vessel's curvature can impact the aneurysm velocity field, leading to a higher degree of three-dimensionality than studied here (Imai *et al.* 2008). As the location of the aneurysm moves away from the apex position, the degree to which the aneurysm flow patterns change will depend on the inertia of the inflow jet induced by the secondary flow at the aneurysm neck opening.

Wall distensibility was not considered in this study, partially due to the growing consensus that compliance in the aneurysmal wall has a smaller influence on intracranial

aneurysm flow than most of the other sources of uncertainty in patient-specific models, such as patient parent vessel flow, segmentation error in the analysis, etc. In a summary of studies comparing the differences between rigid-wall and FSI simulations of cerebral aneurysms, Sarrami-Foroushani *et al.* (2017) showed that the rigid wall assumption often results in a small over-estimation of hemodynamic metrics of the order of 10%, such as WSS, but that the main flow features are preserved. In an experimental analysis of the flow inside untreated cerebral aneurysms, the addition of wall compliance was shown to affect the phase shift of the flow-fields and the development of small-scale flow features near the aneurysm wall that were not found in the rigid model (Tupin *et al.* 2020). However, the characteristics of the primary aneurysm vortex were preserved throughout the cardiac cycle between both rigid and compliant models. By not accounting for the wall-motion in this study, the magnitude of the computed metrics shown here may be slightly over-estimated, and there may exist a shift in the separation time that is not represented here, but the primary findings of the dependence of inflow velocity, vortex direction, and separation time on De are robust to the effect of this patient-specific factor.

The analysis in this study focuses on the velocity field inside the aneurysm and on Eulerian metrics. However, the formation of a stable aneurysm thrombus depends on a number of factors not entirely predicted by the metrics presented, including the biomechanical signaling processes that occur between the aneurysm wall and the detailed platelet dynamics necessary for clot formation, growth and stabilitzation (Rajah *et al.* 2017; Ngoepe *et al.* 2018). A number of researchers are attempting to correlate metrics that capture these processes, including wall shear stress (Mut *et al.* 2015; Paliwal *et al.* 2017) and platelet residence time and shear history (Marsh *et al.* 2020), with the outcome of patients treated by FDS. Efforts are also ongoing to incorporate models of thrombus formation into computational studies of idealized aneurysms and providing new insights into the detailed mechanisms of successful aneurysm occlusion (Ngoepe *et al.* 2018). While the bulk velocity and vorticity fields presented here govern the fluid mechanics inside the aneurysmal cavity and at the wall, and, thus, the residence-time inside the aneurysm cavity, the Eulerian representation of the aneurysm flowfield cannot contain the full history of platelet stress/signaling as Lagrangian metrics can (Marsh *et al.* 2020). This study provides a first step in the full description of intra-aneurysmal hemodynamics, a full parametric (for all three fluid dynamics parameters) characterization of the bulk flow dynamics in FDS-treated cerebral aneurysms, providing new insights on how to understand the limitations of FDS treatment in the context of fundamental fluid dynamics.

Understanding the failure modes of current endovascular aneurysm treatments will enable the development of improved treatment modalities in the future, and may help clinicians prescribe the treatment with the highest likelihood of success. In this work, we have shown that the flow entering sidewall aneurysms treated with FDS depends significantly on the parent vessel De. At high values of De, the efficacy of FDS therapy may be significantly impaired, and other treatment options, such as multiple FDSs or a coil-embolization may have a higher likelihood of treatment success.

Acknowledgements

This work has been financially supported by the NIH/NINDS (grant 1R03NS078539 and 1R01NS088072). This work was also supported by an unrestricted grant in the form of the pipeline devices to our academic institution from Medtronic Inc., which had no role in the experimental design, data analysis or scholarship of this work.

REFERENCES

Adeeb, N., Moore, J.M., Wirtz, M., Griessenauer, C.J., Foreman, P.M., Shallwani, H., Gupta, R., Dmytriw, A.A., Motiei-Langroudi, R., Alturki, A., Harrigan, M.R., Siddiqui, A.H., Levy, E.I., Thomas, A.J. & Ogilvy, C.S. 2017 Predictors of Incomplete Occlusion following Pipeline Embolization of Intracranial Aneurysms: Is It Less Effective in Older Patients? *American Journal of Neuroradiology* **38** (12), 2295–2300.

Aenis, M., Stancampiano, A. P., Wakhloo, A. K. & Lieber, B. B. 1997 Modeling of Flow in a Straight Stented and Nonstented Side Wall Aneurysm Model. *Journal of Biomechanical Engineering* **119** (2), 206–212.

Asgharzadeh, Hafez & Borazjani, Iman 2016 Effects of Reynolds and Womersley Numbers on the Hemodynamics of Intracranial Aneurysms. *Computational and Mathematical Methods in Medicine* **2016**, 1–16.

Augsburger, Luca, Farhat, Mohamed, Reymond, Philippe, Fonck, Edouard, Kulcsar, Zsolt, Stergiopulos, Nikos & Rüfenacht, Daniel A. 2009 Effect of Flow Diverter Porosity on Intraaneurysmal Blood Flow. *Clinical Neuroradiology* **19** (3), 204–214.

Babiker, M. H., Gonzalez, L. F., Ryan, J., Albuquerque, F., Collins, D., Elvikis, A. & Frakes, D. H. 2012 Influence of stent configuration on cerebral aneurysm fluid dynamics. *Journal of Biomechanics* **45** (3), 440–447.

Bovendeerd, P. H. M., Steenhoven, A. A. Van, Vosse, F. N. Van De & Vossers, G. 1987 Steady entry flow in a curved pipe. *Journal of Fluid Mechanics* **177**, 233–246.

Brinjikji, W., Cloft, H.J., Fiorella, D., Lanzino, G. & Kallmes, D. F 2013 Estimating the proportion of intracranial aneurysms likely to be amenable to treatment with the pipeline embolization device. *Journal of NeuroInterventional Surgery* **5** (1), 45–48.

Cantón, G., Levy, D. I., Lasheras, J. C. & Nelson, P. K. 2005*a* Flow changes caused by the sequential placement of stents across the neck of sidewall cerebral aneurysms **103** (3), 891–902.

Cantón, G., Levy, D. I., Lasheras, J. C. & Nelson, P. K. 2005*b* Hemodynamic changes due to stent placement in bifurcating intracranial aneurysms **103** (1), 146–155.

Cebral, J.R. & Raschi, M. 2013 Suggested Connections Between Risk Factors of Intracranial Aneurysms: A Review. *Annals of Biomedical Engineering* **41** (7), 1366–1383.

Chen, Junfan, Zhang, Yisen, Tian, Zhongbin, Li, Wenqiang, Zhang, Qianqian, Zhang, Ying, Liu, Jian & Yang, Xinjian 2019 Relationship between haemodynamic changes and outcomes of intracranial aneurysms after implantation of the pipeline embolisation device: a single centre study. *Interventional Neuroradiology* **25** (6), 671–680.

Damiano, R. J., Ma, Ding, Xiang, Jianping, Siddiqui, Adnan H., Snyder, Kenneth V. & Meng, Hui 2015 Finite element modeling of endovascular coiling and flow diversion enables hemodynamic prediction of complex treatment strategies for intracranial aneurysm. *Journal of Biomechanics* **48** (12), 3332–3340.

Hathcock, James J. 2006 Flow Effects on Coagulation and Thrombosis. *Arteriosclerosis, Thrombosis, and Vascular Biology* **26** (8), 1729–1737.

Higdon, J. J. L. 1985 Stokes flow in arbitrary two-dimensional domains: shear flow over ridges and cavities. *Journal of Fluid Mechanics* **159** (-1), 195.

Imai, Y., Sato, K, Ishikawa, T. & Yamaguchi, T. 2008 Inflow into Saccular Cerebral Aneurysms at Arterial Bends. *Annals of Biomedical Engineering* **36** (9), 1489–1495.

Johnston, S. C., Selvin, S. & Gress, D. R. 1998 The burden, trends, and demographics of mortality from subarachnoid hemorrhage. *Neurology* **50** (5), 1413–1418.

Kim, Minsuok, Taulbee, Dale B., Tremmel, Markus & Meng, Hui 2008 Comparison of Two Stents in Modifying Cerebral Aneurysm Hemodynamics. *Annals of Biomedical Engineering* **36** (5), 726–741.

Kulcsár, Z., Augsburger, L., Reymond, P., Pereira, V. M., Hirsch, S., Mallik, A. S., Millar, J., Wetzel, S. G., Wanke, I. & Rüfenacht, D. A. 2012 Flow diversion treatment: intra-aneurismal blood flow velocity and WSS reduction are parameters to predict aneurysm thrombosis. *Acta Neurochirurgica* **154** (10), 1827–1834.

Lasheras, J. C. 2007 The Biomechanics of Arterial Aneurysms. *Annual Review of Fluid Mechanics* **39** (1), 293–319.

Lieber, Baruch B., Livescu, Veronica, Hopkins, L. N. & Wakhloo, Ajay K. 2002

Particle Image Velocimetry Assessment of Stent Design Influence on Intra-Aneurysmal Flow. *Annals of Biomedical Engineering* **30** (6), 768–777.

Lieber, B. B., Stancampiano, A. P. & Wakhloo, A. K. 1997 Alteration of hemodynamics in aneurysm models by stenting: Influence of stent porosity. *Annals of Biomedical Engineering* **25** (3), 460–469.

Makoyeva, A., Bing, F., Darsaut, T.E., Salazkin, I. & Raymond, J. 2013 The Varying Porosity of Braided Self-Expanding Stents and Flow Diverters: An Experimental Study. *American Journal of Neuroradiology* **34** (3), 596–602.

Maragkos, Georgios A., Ascanio, Luis C., Salem, Mohamed M., Gopakumar, Sricharan, Gomez-Paz, Santiago, Enriquez-Marulanda, Alejandro, Jain, Abhi, Schirmer, Clemens M., Foreman, Paul M., Griessenauer, Christoph J., Kan, Peter, Ogilvy, Christopher S. & Thomas, Ajith J. 2020 Predictive factors of incomplete aneurysm occlusion after endovascular treatment with the Pipeline embolization device. *Journal of Neurosurgery* **132** (5), 1598–1605.

Marsh, Laurel M. M., Barbour, Michael C., Chivukula, Venkat Keshav, Chassagne, Fanette, Kelly, Cory M., Levy, Samuel H., Kim, Louis J., Levitt, Michael R. & Aliseda, Alberto 2020 Platelet Dynamics and Hemodynamics of Cerebral Aneurysms Treated with Flow-Diverting Stents. *Annals of Biomedical Engineering* **48** (1), 490–501.

McAuliffe, W., Wycoco, V., Rice, H., Phatouros, C., Singh, T.J. & Wenderoth, J. 2012 Immediate and Midterm Results following Treatment of Unruptured Intracranial Aneurysms with the Pipeline Embolization Device. *American Journal of Neuroradiology* **33** (1), 164–170.

Meng, H., Tutino, V.M., Xiang, J. & Siddiqui, A. 2014 High WSS or Low WSS? Complex Interactions of Hemodynamics with Intracranial Aneurysm Initiation, Growth, and Rupture: Toward a Unifying Hypothesis. *American Journal of Neuroradiology* **35** (7), 1254–1262.

Morales, H.G., Bonnefous, O., Geers, A.J., Brina, O., Pereira, V.M., Spelle, L., Moret, J. & Larrabide, I. 2016 Does Arterial Flow Rate Affect the Assessment of Flow-Diverter Stent Performance? *American Journal of Neuroradiology* **37** (12), 2293–2298.

Mut, F., Raschi, M., Scrivano, E., Bleise, C., Chudyk, J., Ceratto, R., Lylyk, P. & Cebral, J.R. 2015 Association between hemodynamic conditions and occlusion times after flow diversion in cerebral aneurysms. *Journal of NeuroInterventional Surgery* **7** (4), 286–290.

Ngoepe, Malebogo N., Frangi, Alejandro F., Byrne, James V. & Ventikos, Yiannis 2018 Thrombosis in Cerebral Aneurysms and the Computational Modeling Thereof: A Review. *Frontiers in Physiology* **9**, 306.

Paliwal, N., Damiano, R.J., Davies, J.M., Siddiqui, A.H. & Meng, H. 2017 Association between hemodynamic modifications and clinical outcome of intracranial aneurysms treated using flow diverters. p. 101352F. Orlando, Florida, United States.

Rajah, Gary, Narayanan, Sandra & Rangel-Castilla, Leonardo 2017 Update on flow diverters for the endovascular management of cerebral aneurysms. *Neurosurgical Focus* **42** (6), E2.

Rayepalli, S., Gupta, R., Lum, C., Majid, A. & Koochesfahani, M. 2013 The Impact of Stent Strut Porosity on Reducing Flow in Cerebral Aneurysms: Stent Strut Porosity in Reducing Flow. *Journal of Neuroimaging* **23** (4), 495–501.

Sarrami-Foroushani, Ali, Lassila, Toni & Frangi, Alejandro F. 2017 Virtual endovascular treatment of intracranial aneurysms: models and uncertainty: Virtual endovascular treatment of intracranial aneurysms. *Wiley Interdisciplinary Reviews: Systems Biology and Medicine* **9** (4), e1385.

Sforza, D. M., Putman, C. M. & Cebral, Juan R. 2009 Hemodynamics of Cerebral Aneurysms. *Annual Review of Fluid Mechanics* **41** (1), 91–107.

Sobey, Ian J. 1980 On flow through furrowed channels. Part 1. Calculated flow patterns. *Journal of Fluid Mechanics* **96** (01), 1.

Su, T., Reymond, P., Brina, O., Bouillot, P., Machi, P., Delattre, B.M.A., Jin, L., Lövblad, K.O. & Vargas, M.I. 2020 Large Neck and Strong Ostium Inflow as the Potential Causes for Delayed Occlusion of Unruptured Sidewall Intracranial Aneurysms Treated by Flow Diverter. *American Journal of Neuroradiology* **41** (3), 488–494.

Tomaiuolo, Maurizio, Brass, Lawrence F. & Stalker, Timothy J. 2017 Regulation of Platelet Activation and Coagulation and Its Role in Vascular Injury and Arterial Thrombosis. *Interventional Cardiology Clinics* **6** (1), 1–12.

Tupin, Simon, Saqr, Khalid M. & Ohta, Makoto 2020 Effects of wall compliance on multiharmonic pulsatile flow in idealized cerebral aneurysm models: comparative PIV experiments. *Experiments in Fluids* **61** (7), 164.

Wang, Chao, Tian, Zhongbin, Liu, Jian, Jing, Linkai, Paliwal, Nikhil, Wang, Shengzhang, Zhang, Ying, Xiang, Jianping, Siddiqui, Adnan H., Meng, Hui & Yang, Xinjian 2016 Flow diverter effect of LVIS stent on cerebral aneurysm hemodynamics: a comparison with Enterprise stents and the Pipeline device. *Journal of Translational Medicine* **14** (1), 199.